J|A|C|S ARTICLES

Published on Web 02/26/2009

Enhanced Thermoelectric Performance in Barium and Indium Double-Filled Skutterudite Bulk Materials via Orbital Hybridization Induced by Indium Filler

Wenyu Zhao, Ping Wei, Qingjie Zhang,* Chunlei Dong, Lisheng Liu, and Xinfeng Tang

State Key Laboratory of Advanced Technology for Materials Synthesis and Processing, Wuhan University of Technology, Wuhan 430070, China

Received November 13, 2008; E-mail: zhangqj@whut.edu.cn

Abstract: Maximizing the thermoelectric figure-of-merit (ZT) is a challenge owing to the conflicting combination of material properties. We explored simultaneously enhancing the power factor and reducing the thermal conductivity through filling In in Ba-filled skutterudite ($Ba_{0.3}Co_4Sb_{12}$). Two large ZT values of 1.33 and 1.34 have been achieved for $Ba_{0.15}In_{0.16}Co_4Sb_{11.83}$ and $Ba_{0.14}In_{0.23}Co_4Sb_{11.84}$ at 850 K, respectively. The excellent thermoelectric transport properties for $Ba_fIn_sCo_4Sb_{12}$ are supposed to be due to the orbital hybridizations induced by In filler. It was found that the In filler made the $[Sb_4]^{4-}$ rings become bigger and squarer because of an electron transition from Sb to In brought out by the orbital hybridization between In and Sb and that the Ba filler caused the $[Sb_4]^{4-}$ rings to get smaller and squarer because of a reverse electron transition from Ba to Sb induced by a large difference in electronegativities between Ba and Sb. A model of how to form the rectangular $[Sb_4]^{4-}$ ring is presented, and the five chemical states of Sb in $CoSb_3$ are reasonably assigned to different chemical bonds in the model.

1. Introduction

Thermoelectricity is becoming increasingly important in the field of cooling, heating, generating power, and recovering waste heat.[1] The high performance of thermoelectric modules directly depends on the material thermoelectric figure-of-merit $ZT = \alpha^2\sigma T/\kappa$. In this equation, T is the absolute temperature, σ the electrical conductivity, α the Seebeck coefficient, and κ the thermal conductivity ($\kappa = \kappa_E + \kappa_L$ where κ_E is the electronic contribution and κ_L is the lattice contribution). A good thermoelectric material should be perfective combination of high power factor ($\alpha^2\sigma$) with low thermal conductivity.[2] The nanostructures lowering κ and the distortion of electronic density of states enhancing α are at present effective approaches to enlarge ZT.[3,4] However, it is in fact very hard to simultaneously increase $\alpha^2\sigma$ and reduce κ because of the conflicting thermoelectric material properties,[2] though Li et al. reported increasing $\alpha^2\sigma$ and decreasing κ in nanostructured $AgPb_mSbTe_{m+2}$ compounds by annealing treatment.[5]

Skutterudites are being intensely pursued in hopes of developing efficient thermoelectric materials. Extensive reviews of the physical properties of the skutterudites were given by Nolas et al.,[6] Uher,[7] and Sales.[8] Binary skutterudites crystallize in a body-centered cubic structure and have two interstitial voids at the 2*a* positions in the crystal lattice. Filling the oversized voids with foreign atoms such as rare earth elements (La, Ce, Yb, Eu, Nd, and Sm),[9−20] alkaline earth elements (Ba, Sr, and Ca),[21−24] and others (Y, Sn, Tl, Ge, In, and K)[25−31] has been

(1) Bell, L. E. *Science* **2008**, *321*, 1457.
(2) Snyder, G. J.; Toberer, E. S. *Nat. Mater.* **2008**, *8*, 105.
(3) Poudel, B.; Hao, Q.; Ma, Y.; Lan, Y. C.; Minnich, A.; Yu, B.; Yan, X.; Wang, D. Z.; Muto, A.; Vashaee, D.; Chen, X. Y.; Liu, J. M.; Dresselhaus, M. S.; Chen, G.; Ren, Z. F. *Science* **2008**, *320*, 634.
(4) Heremans, J. P.; Jovovic, V.; Toberer, E. S.; Saramat, A.; Kurosaki, K.; Charoenphakdee, A.; Yamanaka, S.; Snyder, G. J. *Science* **2008**, *321*, 554.
(5) Zhou, M.; Li, J.-F.; Kita, T. *J. Am. Chem. Soc.* **2008**, *130*, 4527.
(6) Nolas, G. S.; Morelli, D. T.; Tritt, T. M. *Annu. Rev. Mater. Sci.* **1999**, *29*, 89–116.
(7) Uher, C. In *Recent Trends in Thermoelectric Materials Research I, Semiconductors and Semimetals*; Tritt, T. M., Ed.; Academic Press: New York, 2001; Vol. 69, pp 139−253.
(8) Sales, B. C. In *Handbook on the Physics and Chemistry of Rare Earths*; Gschneidner, K. A., Jr., Bünzli, J.-C. C., Pecharsky, V., Eds.; Elsevier: New York, 2003; Vol. 33.
(9) Sales, B. C.; Mandrus, D.; Williams, R. K. *Science* **1996**, *272*, 1325.
(10) Nolas, G. S.; Cohn, J. L.; Slack, G. A. *Phys. Rev. B* **1998**, *58*, 164.
(11) Morelli, D. T.; Meisner, G. P.; Chen, B. X.; Hu, S. Q.; Uher, C. *Phys. Rev. B* **1997**, *56*, 7376.
(12) Chen, B. X.; Xu, J. H.; Uher, C.; Morelli, D. T.; Meisner, G. P.; Fleurial, J.-P.; Caillat, T.; Borshchevsky, A. *Phys. Rev. B* **1997**, *55*, 1476.
(13) Meisner, G. P.; Morelli, D. T.; Hu, S.; Yang, J.; Uher, C. *Phys. Rev. Lett.* **1998**, *80*, 3551.
(14) Nolas, G. S.; Kaeser, M.; Littleton, R. T.; Tritt, T. M. *Appl. Phys. Lett.* **2000**, *77*, 1855.
(15) Dilley, N. R.; Bauer, E. D.; Maple, M. B.; Sales, B. C. *J. Appl. Phys.* **2000**, *88*, 1948.
(16) Lamberton, G. A., Jr.; Bhattacharya, S.; Littleton, R. T., IV.; Kaeser, M. A.; Tedstrom, R. H.; Tritt, T. M.; Yang, J.; Nolas, G. S. *Appl. Phys. Lett.* **2002**, *80*, 598.
(17) Yang, J.; Morelli, D. T.; Meisner, G. P.; Chen, W.; Dyck, J. S.; Uher, C. *Phys. Rev. B* **2003**, *67*, 165207.
(18) Zhai, P. C.; Zhao, W. Y.; Li, Y.; Liu, L. S.; Tang, X. F.; Zhang, Q. J.; Niino, M. *Appl. Phys. Lett.* **2006**, *89*, 052111.
(19) Yang, C. P.; Wang, H.; Iwasa, K.; Kohgi, M.; Sugawara, H.; Sato, H. *Appl. Phys. Lett.* **2007**, *90*, 102503.
(20) Sun, P.; Nakanishi, Y.; Nakamura, M.; Yoshizawa, M.; Ohashi, M.; Oomi, G.; Sekine, C.; Shirotani, I. *Phys. Rev. B* **2007**, *75*, 054114.
(21) Chen, L. D.; Kawahara, T.; Tang, X. F.; Goto, T.; Hirai, T.; Dyck, J. S.; Chen, W.; Uher, C. *J. Appl. Phys.* **2001**, *90*, 1864.

confirmed to be an effective way to reduce κ_L. High ZT values have been reported for both *p*- and *n*-type single-filled skutterudite materials.[9,21−23] Some experimental data show that the ZT values of double-filled skutterudite compounds such as $Ce_mLa_nFeCo_3Sb_{12}$,[32] $Ca_mCe_nFe_xCo_{4-x}Sb_{12}$,[33] and $Ba_xR_yCo_4Sb_{12}$ (R = La, Ce, Sr, and Yb)[34,35] were bigger than those of single-filled ones. Yang et al. predicted the significant reduction in the κ_L for multiple-filled skutterudite compounds.[34] We had investigated the high-temperature transport properties of Ba and In double-filled skutterudites $Ba_xIn_yCo_4Sb_{12-z}$ with maximum ZT of 1.19 synthesized with nominal compositions $Ba_{0.3-k}In_kCo_4Sb_{12}(0 \le k \le 0.3)$ and found that the double filling was indeed more efficient in lowering κ_L than single-filled skutterudties.[36] The mechanism of the κ_L decrease induced by fillers for single- and double-filled skutterudite materials is in question. It was generally accepted that the κ_L suppression was due to the strong phonon resonance scattering because of the individual rattling of the fillers.[9,37] However, the new neutron-spectroscopy experiments seemed to give an unambiguous evidence of a quasi-harmonic coupling between the fillers and the host lattice in filled skutterudites.[38] Christensen et al. deemed that the effect of the rattler in $Ba_8Ga_{16}Ge_{30}$ was to flatten the phonon bands rather than to provide a strong phonon scattering mechanism.[39] In this paper, we found that filling In in Ba-filled skutterudite ($Ba_{0.3}Co_4Sb_{12}$) not only remarkably reduced the thermal conductivity but also significantly enhanced the $\alpha^2\sigma$ for $Ba_rIn_sCo_4Sb_{12}$ bulk materials with higher ZTs, up to 1.34, fabricated with nominal compositions $Ba_{0.3}In_mCo_4Sb_{12}$ ($0 \le m \le 0.3$, $\Delta m = 0.05$), and we further investigated the mechanism of In-triggered thermoelectric performance enhancement in Ba-filled skutterudite. The quantitative analysis of experimental data from X-ray photoelectron spectroscopy (XPS) revealed the correlation between the excellent thermoelectric transport properties for $Ba_rIn_sCo_4Sb_{12}$ and the orbital hybridizations induced by In filler.

(22) Dyck, J. S.; Chen, W.; Uher, C.; Chen, L. D.; Tang, X. F.; Hirai, T. *J. Appl. Phys.* **2002**, *91*, 3698.
(23) Puyet, M.; Dauscher, A.; Lenoir, B.; Dehmas, M.; Stiewe, C.; Müller, E.; Hejtmanek, J. *J. Appl. Phys.* **2005**, *97*, 083712.
(24) Zhao, X. Y.; Shi, X.; Chen, L. D.; Zhang, W. Q.; Zhang, W. B.; Pei, Y. Z. *J. Appl. Phys.* **2006**, *99*, 053711.
(25) Tang, X. F.; Zhang, Q. J.; Chen, L. D.; Goto, T.; Hirai, T. *J. Appl. Phys.* **2005**, *97*, 093712.
(26) Nolas, G. S.; Takizawa, H.; Endo, T.; Sellinschegg, H.; Johnson, D. C. *Appl. Phys. Lett.* **2000**, *77*, 52.
(27) Sales, B. C.; Chakoumakos, B. C.; Mandrus, D. *Phys. Rev. B* **2000**, *61*, 2475.
(28) Nolas, G. S.; Kendziora, C. A.; Takizawa, H. *J. Appl. Phys.* **2003**, *94*, 7440.
(29) He, T.; Chen, J. Z.; Rosenfeld, H. D.; Subramanian, M. A. *Chem. Mater.* **2006**, *18*, 759.
(30) Zhang, W.; Shi, X.; Mei, Z. G.; Xu, Y.; Chen, L. D.; Yang, J.; Meisner, G. P. *Appl. Phys. Lett.* **2006**, *89*, 112105.
(31) Pei, Y. Z.; Chen, L. D.; Zhang, W.; Shi, X.; Bai, S. Q.; Zhao, X. Y.; Mei, Z. G.; Li, X. Y. *Appl. Phys. Lett.* **2006**, *89*, 221107.
(32) Lu, Q. M.; Zhang, J. X.; Zhang, X.; Liu, Y. Q.; Liu, D. M.; Zhou, M. L. *J. Appl. Phys.* **2005**, *98*, 106107.
(33) Tang, X. F.; Li, H.; Zhang, Q. J.; Niino, M.; Goto, T. *J. Appl. Phys.* **2006**, *100*, 123702.
(34) Yang, J.; Zhang, W.; Bai, S. Q.; Mei, Z.; Chen, L. D. *Appl. Phys. Lett.* **2007**, *90*, 192111.
(35) Shi, X.; Kong, H.; Li, C.-P.; Uher, C.; Yang, J.; Salvador, J. R.; Wang, H.; Chen, L.; Zhang, W. *Appl. Phys. Lett.* **2008**, *92*, 182101.
(36) Zhao, W. Y.; Dong, C. L.; Wei, P.; Guan, W.; Liu, L. S.; Zhai, P. C.; Tang, X. F.; Zhang, Q. J. *J. Appl. Phys.* **2007**, *102*, 113708.
(37) Keppens, V.; Mandrus, D.; Sales, B. C.; Chakoumakos, B. C.; Day, P.; Coldea, R.; Maple, M. B.; Gajewski, D. A.; Freeman, E. J.; Bennington, S. *Nature* **1998**, *395*, 876.
(38) Koza, M. M.; Johnson, M. R.; Viennois, R.; Mutka, H.; Girard, L.; Ravot, D. *Nat. Mater.* **2008**, *7*, 805.
(39) Christensen, M.; Abrahamsen, A. B.; Christensen, N. B.; Juranyi, F.; Andersen, N. H.; Lefmann, K.; Andreasson, J.; Bahl, C. R. H.; Iversen, B. B. *Nat. Mater.* **2008**, *7*, 811.

2. Experimental Section

2.1. Synthesis. The highly pure metals of Ba (99.9%, plate), In (99.99%, powder), Sb (99.999%, powder), and Co (99.9%, powder) were used as the starting materials. The mixtures of these starting materials with nominal compositions $Ba_{0.3}In_mCo_4Sb_{12}$ ($0 \le m \le 0.3$, $\Delta m = 0.05$) were loaded into a graphite crucible and then put into a silica tube. The tube was sealed under vacuum and transferred into a programmable furnace, which was heated up to 1373 K for 24 h, followed by quenching in oil, and then was annealed at 933 K for 120 h. The annealed products were ground into fine powder and then sintered into polycrystalline bulk materials by spark plasma sintering (SPS) (Dr Sinter: SPS-1050) method at 903 K for 7 min in a graphite die. The heat treatment and SPS parameters were confirmed to be suitable for fabricating the Ba and In double-filled skutterudite bulk materials from highly pure metals by our previous studies.[36]

2.2. X-ray Diffraction and Electron Microscopy Analysis. The constituent phases of all resultant samples were determined by powder X-ray diffraction (XRD) by using Cu Kα radiation (PANalytical X' Pert PRO). The chemical compositions were quantitatively analyzed by using JXA-8100 electron probe microanalysis (EPMA). The operation conditions of the accelerating voltage, specimen current, beam diameter, and counting time were kept at 25 kV, 20 nA, OFF, and 20 s, respectively. The backscattered-electron images were observed by using JSM-5610LV scanning electron microscopy to evaluate whether the SPS bulk materials exist the impurity.

2.3. XPS. XPS measurements were performed on VG Multilab 2000 X-ray photoelectron spectrometer by using monochromatic Al Kα line (photo energy 1486.6 eV) and a 180° hemispherical analyzer in the constant-resolution mode (pass energy 25 eV for the core-level spectra and 100 eV for wide-scan spectra). The energy resolution (full width at half-maximum) was 0.47 eV for Cu $2p_{3/2}$ core level in the analyzer mode with the pass energy of 25 eV. The operation conditions of energy step size and spot size were kept 0.05 eV and OFF, respectively. Samples were polished and loaded into the ultrahigh vacuum analyzer chamber, then cleaned by argon-ion sputtering until no traces of contamination (mainly core lines of carbon and oxygen). The binding energies of Co 2*p* and Ba 3*d* core levels were too close to collect individually their X-ray photoelectron spectra. Therefore, X-ray photoelectron spectra of Co 3*p* core level were recorded to investigate the effect of In filler on the electron structures of Co in $Ba_rIn_sCo_4Sb_{12}$.

2.4. Carrier Transport Properties. The Hall coefficient (R_H) and electrical resistivity (ρ) at room temperature were measured by the van der Pauw method by using the Hall measurement system (Accent 5500). The carrier concentration (n) and Hall mobility (μ_H) were calculated by using the formula $n = 1/(R_H q)$ and $\mu_H = R_H/\rho$, respectively, where q is the carrier charge. The high-temperature σ and α were measured with the standard four-probe method (Sinkuriko: ZEM-1) in Ar atmosphere.

2.5. Thermal Conductivity. κ was calculated by using the equation $\kappa = \lambda\rho C_p$, where C_p is the specific heat capacity, ρ is the bulk density of the material, and λ is the thermal diffusivity coefficient. λ was measured by a laser-flash technique (Netzsch LFA 427) in a flowing Ar atmosphere. C_p was measured by using differential scanning calorimeter. ρ was obtained by the Archimedes method. κ_L was obtained by subtracting the electrical contribution from κ by using the equation $\kappa_L = \kappa - \kappa_E$. Here, κ_E is expressed by the Wiedemann−Franz $\kappa_E = \sigma LT$, where L is the Lorenz number.

3. Results

3.1. Structural and Compositional Characterizations. XRD patterns of $Ba_rIn_sCo_4Sb_{12}$ bulk materials are shown in Figure

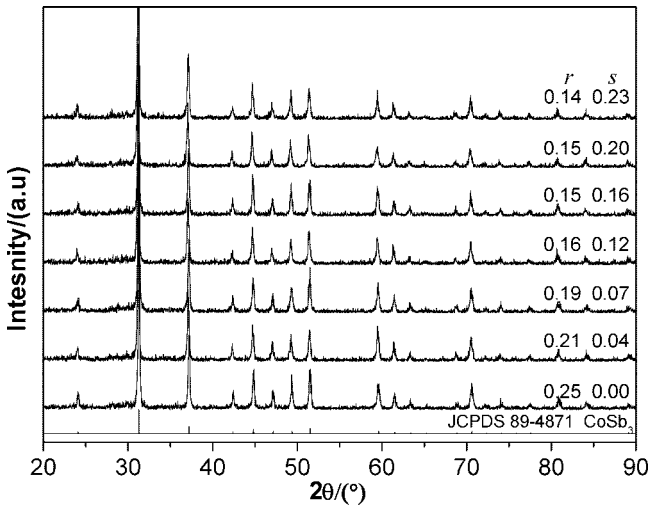

Figure 1. XRD patterns of $Ba_rIn_sCo_4Sb_{12}$ bulk materials fabricated with nominal compositions $Ba_{0.3}In_mCo_4Sb_{12}$ ($0 \le m \le 0.3$, $\Delta m = 0.05$)

1. It can be seen that all the samples except $Ba_{0.14}In_{0.23}Co_4Sb_{12}$ are composed of single-phase compound with skutterudite structure. This indicates that the Ba and In double-filled skutterudite structure is stable thermodynamically. Rietveld refinement from high-resolution synchrotron data for $In_sCo_4Sb_{12}$[29] confirmed that the In could fill in the Sb-icosahedron voids and was loosely bound with the adjacent atoms. Rietveld refinement from XRD data for $Ba_xIn_yCo_4Sb_{12-z}$ indicated that the In filler still filled in the Sb-icosahedron voids although the thermal vibration parameter (U_{iso}) for In filler was bigger by an order of magnitude than that for Ba filler.[36] Some weak peaks were observed in the XRD pattern of the sample for $Ba_{0.14}In_{0.23}Co_4Sb_{12}$, which were attributed to the characteristic diffraction peaks of In-containing impurity phase such as InSb.

The EPMA compositions of Ba and In double-filled skutterudite compounds $Ba_rIn_sCo_4Sb_{12}$ are listed in Table 1. Notice that the filling fractions of Ba decreased gradually with increasing the filling fractions of In whereas the total filling fractions increased, as shown in Figure 2. This indicates that the In filler occupied the Sb-icosahedron voids more easily than the Ba filler. The actual filling fractions of Ba and In derived from EPMA are less than their nominal compositions, which is consistent with our previous result.[36] This is presumably caused by both the sublimation of Ba and In during melting and the formation of a Ba-containing impurity phase ($BaSb_3$) and an In-containing impurity phase (InSb). The actual filling fraction of In for nominal composition $Ba_{0.3}In_{0.3}Co_4Sb_{12}$ is only 0.23. This is because the filling fraction limit of In in the skutterudite structure is about 0.22, as pointed out in refs 29 and 36.

3.2. Charge Transport Properties. The charge transport properties for $Ba_rIn_sCo_4Sb_{12}$ bulk materials at room temperature are listed in Table 1. Hall coefficients of all samples are negative, exhibiting that Ba and In fillers acted as donor impurity in the skutterudite structure. R_H and μ_H of $Ba_{0.21}In_{0.04}Co_4Sb_{11.93}$ significantly increased compared to that of $Ba_{0.25}Co_4Sb_{11.91}$, implying a great prolongation in the relaxation time of carriers τ according to the formula $\tau = m^*\mu_H/q$, where m^* is the effective mass of the carrier. The reduction in the n of $Ba_{0.21}In_{0.04}Co_4Sb_{11.93}$ compared to that of $Ba_{0.25}Co_4Sb_{11.91}$ was due to the lower charge provided by In filler than that provided by Ba filler. In general, each Ba impurity provided two electrons for the skutterudite structure, whereas each In impurity provided one electron, as pointed out in ref 36. R_H and μ_H of $Ba_rIn_sCo_4Sb_{12}$ except $Ba_{0.21}In_{0.04}Co_4Sb_{11.93}$ gradually decreased as r decreased and s increased. In addition to the enhancement in m^*, another possible reason for the reductions in R_H and μ_H is the stronger phonon scattering of In filler than that of Ba filler because of the larger U_{iso} of In filler.[36] The n of $Ba_rIn_sCo_4Sb_{12}$ except $Ba_{0.21}In_{0.04}Co_4Sb_{11.93}$ increased monotonically as r decreased and s increased. Therefore, the amount of charge provided by Ba and In fillers in $Ba_rIn_sCo_4Sb_{12}$ compounds, which is generally considered as a key factor to change n, should exhibit a similar evolution to that of n as r decreased and s increased. However, the calculated amount of charges, based on the filling fractions of Ba and In and the electron quantities provided by them, in fact decreased first and then increased as r decreased and s increased. We think that the reason for this is that there must be some other mechanisms in the $Ba_rIn_sCo_4Sb_{12}$ system that result in the gradual increase in n with decreasing r and increasing s besides the charges provided by Ba and In filler.

The temperature dependence of electrical conductivity for $Ba_rIn_sCo_4Sb_{12}$ is shown in Figure 3a. The gradual reduction in the σ of $Ba_rIn_sCo_4Sb_{12}$ with increasing the temperature in the range of 300−700 K can be explained in terms of the enhancement in the scattering effect of the carriers and phonons on crystal lattice. The gradual increase in σ of $Ba_rIn_sCo_4Sb_{12}$ at a certain temperature with decreasing r and increasing s must be due to the augmentation of n because of the reduction of the μ_H in the formula $\sigma = ne\mu_H$. $Ba_{0.15}In_{0.16}Co_4Sb_{11.83}$ exhibits the most excellent thermoelectric transport behavior. The anomalous behavior is possibly related to the presence of a localized state in the gap. Ahmad et al. suggested that three valence electrons of In impurity in PbTe had the same electronic configuration, two electrons occupied a localized state below the valence-band maximum and one electron occupied a localized state in the gap, and that the electron in the gap could annihilate minority carriers and also trap electrons, which could be excited to the conduction band at high temperatures and lead to enhanced thermoelectric behavior.[40] The biggest σ for $Ba_{0.14}In_{0.23}Co_4Sb_{11.84}$ is attributed to the contribution of In-containing impurity phase such as n-type semiconductor compound InSb with high σ.[41]

The temperature dependence of Seebeck coefficients for $Ba_rIn_sCo_4Sb_{12}$ is displayed in Figure 3b. All samples have negative Seebeck coefficients, indicating that the majority carriers are electrons. The absolute values of α for $Ba_{0.25}Co_4Sb_{11.91}$ increased with temperature and then decreased when the temperature was over 700 K. The change of α implied a transformation from semimetallic to semiconducting behavior at 700 K. Because the electron transition from the valence band to the conduction band would bring out the same amount of holes when the temperature was over 700 K, the negative effect of the holes caused the reduction in the absolute values of α. However, the behavior was weakened by In filler and even vanished when $r \le 0.15$ and $s \ge 0.16$. Comparable to $Ba_{0.25}Co_4Sb_{11.91}$, the absolute value of α for $Ba_{0.21}In_{0.04}Co_4Sb_{11.93}$ remarkably increased whereas σ increased significantly. As a consequence, the $\alpha^2\sigma$ for $Ba_{0.21}In_{0.04}Co_4Sb_{11.93}$ is far more than that for $Ba_{0.25}Co_4Sb_{11.91}$. The absolute values of α for $Ba_rIn_sCo_4Sb_{12}$ except for $Ba_{0.21}In_{0.04}Co_4Sb_{11.93}$ at a certain temperature decreased with decreasing r and increasing s. The evolution can be explained in terms of the compromise between α and n in thermoelectric materials, see eq 1. With the above

(40) Ahmad, S.; Hoang, K.; Mahanti, S. D. *Phys. Rev. Lett.* **2006**, *96*, 056403.
(41) Zawadski, W. *Adv. Phys.* **1974**, *23*, 435.

Table 1. Compositions and Charge-Transport Properties of Ba and In Double-Filled Skutterudites at Room Temperature

nominal composition	EPMA composition	Hall coefficient (10^{-2} cm$^3\cdot$C^{-1})	carrier mobility (cm$^2\cdot$V$^{-1}\cdot$s^{-1})	carrier concentration (10^{20} cm^{-3})	electrical conductivity (10^5 S$\cdot$m^{-1})
$Ba_{0.30}Co_4Sb_{12}$	$Ba_{0.25}Co_4Sb_{11.91}$	−3.08	44.12	−2.03	1.312
$Ba_{0.30}In_{0.05}Co_4Sb_{12}$	$Ba_{0.21}In_{0.04}Co_4Sb_{11.93}$	−3.62	54.81	−1.73	1.434
$Ba_{0.30}In_{0.10}Co_4Sb_{12}$	$Ba_{0.19}In_{0.07}Co_4Sb_{11.85}$	−3.54	54.69	−1.77	1.619
$Ba_{0.30}In_{0.15}Co_4Sb_{12}$	$Ba_{0.16}In_{0.12}Co_4Sb_{11.85}$	−2.90	48.26	−2.15	1.721
$Ba_{0.30}In_{0.20}Co_4Sb_{12}$	$Ba_{0.15}In_{0.16}Co_4Sb_{11.83}$	−2.34	42.17	−2.70	1.829
$Ba_{0.30}In_{0.25}Co_4Sb_{12}$	$Ba_{015}In_{0.20}Co_4Sb_{11.84}$	−2.19	36.02	−2.85	1.810
$Ba_{0.30}In_{0.30}Co_4Sb_{12}$	$Ba_{0.14}In_{0.23}Co_4Sb_{11.84}$	−1.31	24.90	−4.81	1.944

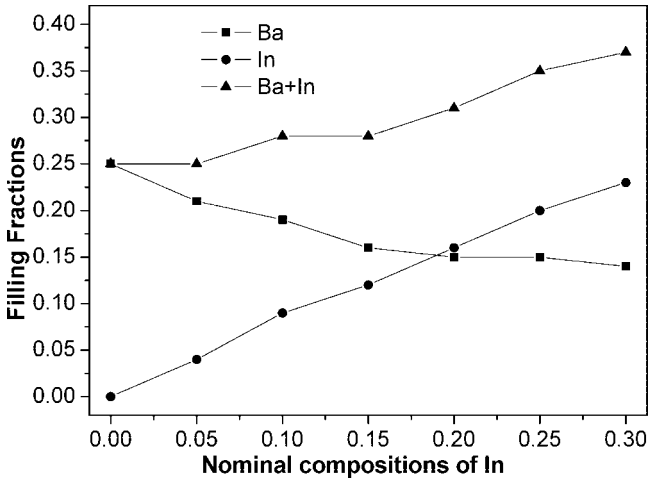

Figure 2. Filling fractions of Ba and In and total fractions in $Ba_rIn_sCo_4Sb_{12}$

values of σ and α, $\alpha^2\sigma$ for all samples were calculated, showing a remarkable enhancement for $Ba_rIn_sCo_4Sb_{12}$ compared to that for $Ba_{0.25}Co_4Sb_{11.91}$. For metals or degenerate semiconductors, α is given by:

$$\alpha = \frac{8\pi^2 k_B^2}{3eh^2} m^* T \left(\frac{\pi}{3n}\right)^{2/3} \quad (1)$$

3.3. Lattice Thermal Conductivity and Thermoelectric Figure of Merit. The temperature dependence of thermal conductivity for $Ba_rIn_sCo_4Sb_{12}$ is shown in Figure 4a. κ of $Ba_rIn_sCo_4Sb_{12}$ was far less than that of $Ba_{0.25}Co_4Sb_{11.91}$. The sample $Ba_{0.15}In_{0.16}Co_4Sb_{11.83}$ showed the lowest κ value of 2.35 W/m K at 675 K. κ_E was calculated by the Wiedemann−Franz law as $\kappa_E = L_0T\sigma$, where the Lorenz number L_0 has a numerical value of 2.0×10^{-8} V^2/K^2 estimated by Dyck et al.[22] κ_L was obtained by subtracting κ_E from κ. The temperature dependences of κ_E and κ_L for $Ba_rIn_sCo_4Sb_{12}$ are shown in Figure 4b and c, respectively. κ_E at a certain temperature increased with decreasing r and increasing s. The increase in κ_E as the temperature rose was attributed to the contribution of the temperature according to the temperature dependence of σ of $Ba_rIn_sCo_4Sb_{12}$. κ_L for $Ba_rIn_sCo_4Sb_{12}$ was much lower than that of $Ba_{0.25}Co_4Sb_{11.91}$ and decreased gradually with decreasing r and increasing s, except for $Ba_{0.15}In_{0.16}Co_4Sb_{11.83}$. The lowest κ_L of 0.74 W/m K at 850 K has been obtained for $Ba_{0.14}In_{0.23}Co_4Sb_{11.84}$.

Figure 4d displays ZTs for $Ba_rIn_sCo_4Sb_{12}$ between 300 and 850 K on the basis of the measured σ, α, α, and κ. It is worth noting that the remarkable increase in $\alpha^2\sigma$ and the significant reduction in κ play a key role in enhancing ZTs for $Ba_rIn_sCo_4Sb_{12}$. A promising ZT value of ~1.0 has been obtained for four samples of $Ba_rIn_sCo_4Sb_{12}$ with $r \le 0.16$ and $s \ge 0.12$

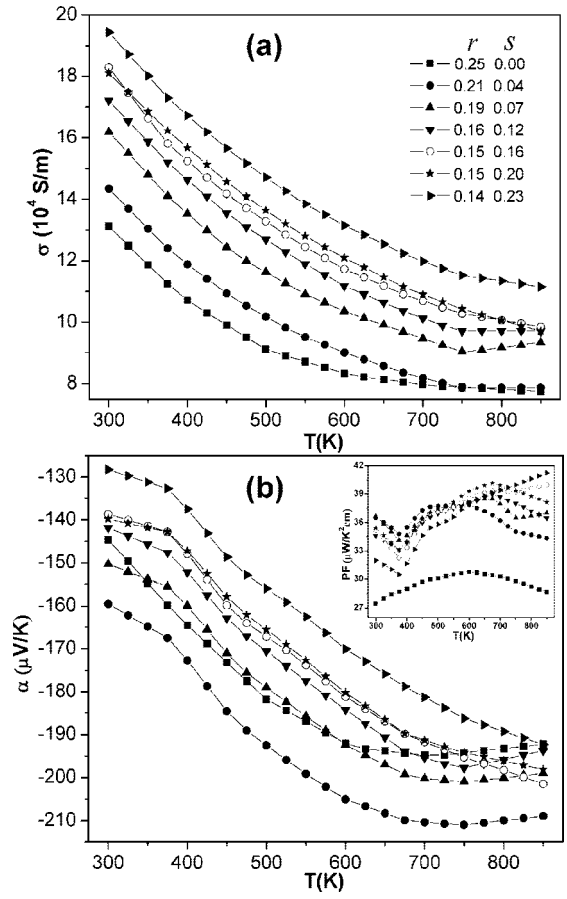

Figure 3. Temperature dependence of (a) electrical conductivity and (b) Seebeck coefficient for $Ba_rIn_sCo_4Sb_{12}$. The inset in panel b shows the temperature dependence of power factor.

at 625 K, which is very close to that of $Ba_{0.08}Yb_{0.09}Co_4Sb_{12.12}$[35] and much higher than that of single Ba-filled skutterudites reported by other authors[21,22] and by us.[36] The ZT for $Ba_rIn_sCo_4Sb_{12}$ increased monotonically with increasing temperature with no hint of reaching a maximum even at 850 K, demonstrating the beneficial effect of In impurity. The nature of the doping effect due to In is as follows: (1) the In filler acts as electron donor and even occupies the Sb-icosahedron voids more easily than the Ba filler; this is the reason that the total filling fractions of Ba and In and σ increased, (2) m^* increases, thereby reducing R_H and μ_H, and (3) κ_L is remarkably reduced. All of these factors help increase the thermoelectric performance. The ZT values in our best two samples ($Ba_{0.15}In_{0.16}Co_4Sb_{11.83}$ and $Ba_{0.14}In_{0.23}Co_4Sb_{11.84}$) are comparable to that of $Ba_{0.08}Yb_{0.09}Co_4Sb_{12.12}$[35] and reach 1.33 and 1.34 at 850 K, respectively. The bigger ZT value of $Ba_{0.14}In_{0.23}Co_4Sb_{11.84}$ than that of $Ba_{0.15}In_{0.20}Co_4Sb_{11.84}$ was attributed to the contribution of In-containing impurity phase InSb to the σ of the sample

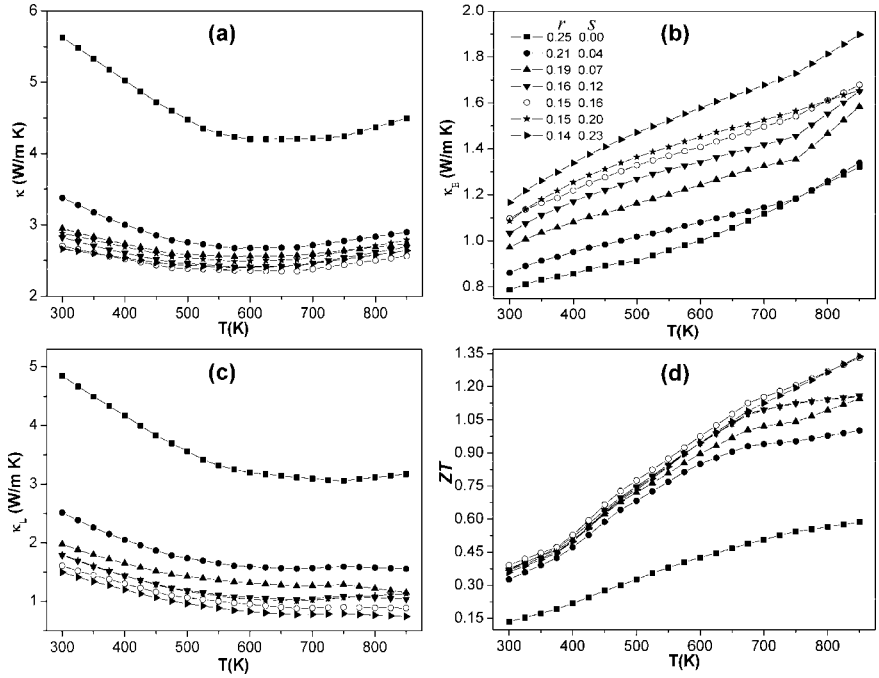

Figure 4. Temperature dependences of (a) thermal conductivity, (b) electronic thermal conductivity, (c) lattice thermal conductivity, and (d) ZT values from 300 to 850 K for $Ba_rIn_sCo_4Sb_{12}$.

$Ba_{0.14}In_{0.23}Co_4Sb_{11.84}$. Compared to the previously reported data with ZT values of at least 0.8 at 800 K for the samples with nominal composition $Ba_{0.3}Co_4Sb_{12}$,[21,22] the lower ZT values of the samples $Ba_{0.25}Co_4Sb_{11.91}$ and $Ba_{0.27}Co_4Sb_{11.84}$[36] were possibly due to the different processes and the difference in the purity of the starting materials.

4. Discussion

4.1. Orbital Hybridization of Valence Electrons and Bonding States in $CoSb_3$. Early work suggested that the skutterudite structure followed the so-called Oftedal's relation ($y + z = 1/2$, where y and z are the atomic coordinates of Sb in $CoSb_3$), which results in squared $[Sb_4]^{4-}$ rings. However, subsequent structural studies revealed that, in the vast majority of filled and unfilled skutterudites, the $[Sb_4]^{4-}$ rings are instead rectangular with short and long Sb−Sb distances alternating within the ring.[42] The 12 p states of four Sb atoms in the $[Sb_4]^{4-}$ ring hybridized with each other, forming four strongly bound ppσ bonding states (split into two close pairs by weak ppπ interactions), four ppσ antibonding states, and two pairs of weakly bound ppπ bonding/antibonding states formed by the orbitals perpendicular to the plane of the $[Sb_4]^{4-}$ ring.[43] The largest distortion of the $[Sb_4]^{4-}$ ring was found in unfilled skutterudites, with the rings becoming squarer as the filling fraction increased.[44] In Raman scattering for $CoSb_3$, the compound had a mode near 150 cm^{-1} and another near 185 cm^{-1}. The higher-energy mode was presumably the stretching of the shorter Sb−Sb bond, and the lower-energy one was the stretching of the longer Sb−Sb bond.[45] Extended Hückel tight-binding (EHTB) calculations for skutterudite-type CoP_3 and NiP_3 indicated that the high-energy region of the valence band was mainly formed by the nonbonding and the bonding π-type molecular orbitals of the $[P_4]^{4-}$ rings, the bottom of the conduction band was mainly formed by ring antibonding molecular orbitals, and the lowest region was due basically to the σ-bonding orbitals of the $[P_4]^{4-}$ rings with large phosphorus 3s contributions.[46,47]

On the basis of available understandings of structural studies and EHTB calculations about skutterudite compounds, a model for describing the orbital hybridizations of Sb and Co and the bonding states in $CoSb_3$ is proposed to explain how to form the rectangular $[Sb_4]^{4-}$ ring. In the model, 5s and $5p_x$ (or $5p_y$ or $5p_z$) orbitals of Sb atom are first hybridized inhomogenously in sp pattern and become two hydribization ones with different energies, e.g., $1 - \beta$ and β, as shown in Figure 5a. The $1 - \beta$ orbital with lower energy and large s contributions is a s-shape nonbonding one. The β orbital is similar to the p-shape bonding one containing a large p contribution. In the rectangular $[Sb_4]^0$ ring, as shown in Figure 5b, the β orbital is superposed face to face with another β one from the most adjacent Sb atom and forms $\beta\beta\sigma$ Sb−Sb bond, the $5p_y$ or $5p_z$ orbital is superposed face to face with another $5p_y$ or $5p_z$ one from the second most adjacent Sb atom and forms ppσ Sb−Sb bond perpendicular to the $\beta\beta\sigma$ Sb−Sb bond, and an additional $5p_z$ or $5p_y$ orbital is superposed by side and forms ppπ bond perpendicular to the rectangular $[Sb_4]^0$ ring. The bond length of the $\beta\beta\sigma$ Sb−Sb bond is shorter than that of the ppσ Sb−Sb one because of the difference in energies between the β orbital and the $5p_y$ or $5p_z$ orbital. As a consequence, the rectangular $[Sb_4]^0$ ring is an

(42) Leithe-Jasper, A.; Schnelle, W.; Rosner, H.; Baenitz, M.; Rabis, A.; Gippius, A. A.; Morozova, E. N.; Borrmann, H.; Burkhardt, U.; Ramlau, R.; Schwarz, U.; Mydosh, J. A.; Grin, Y.; Ksenofontov, V.; Reiman, S. *Phys. Rev. B* **2004**, *70*, 214418.
(43) Singh, D. J.; Mazin, I. I. *Phys. Rev. B* **1997**, *56*, R1650.
(44) Chakoumakos, B. C.; Sales, B. C. *J. Alloys Compd.* **2006**, *407*, 87–93.
(45) Nolas, G. S.; Slack, G. A.; Caillat, T.; Meisner, G. P. *J. Appl. Phys.* **1996**, *79*, 2622.
(46) Jung, D.; Whangbo, M.-H.; Alvarez, S. *Inorg. Chem.* **1990**, *29*, 2252–2255.
(47) Llunell, M.; Alemany, P.; Alvarez, S.; Zhukov, V. P.; Vernes, A. *Phys. Rev. B* **1996**, *53*, 10605–10609.

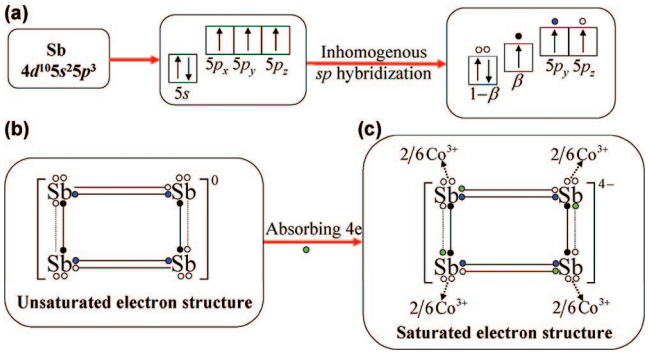

Figure 5. (a) Orbital hybridization for valence electrons of Sb and (b) bond of the rectangular Sb_4 ring in unfilled skutterudite $CoSb_3$.

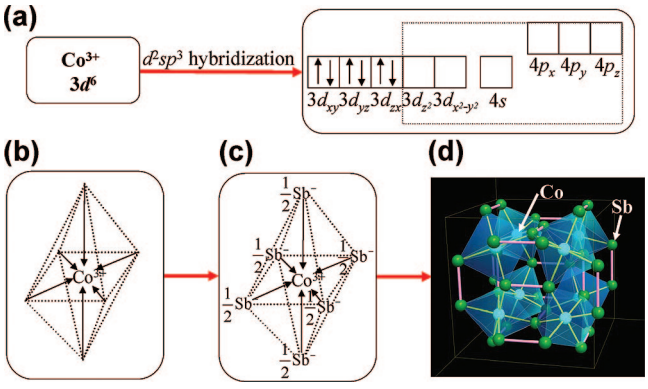

Figure 6. (a) Orbital hybridization for valence electrons of Co^{3+} and (b) bond of octahedron $[CoSb_6]$ in unfilled skutterudite $CoSb_3$.

unsaturated electron structure, because each Sb atom in the ring is a seven-electron configuration. Thus, it can be transformed spontaneously into the $[Sb_4]^{4-}$ ring with saturated electron structure as shown in Figure 5c by absorbing four electrons. For the unfilled skutterudite $CoSb_3$, four foreign electrons come from eight Co atoms, which are provided by sharing the vertices of $[CoSb_6]$ octahedra as shown in Figure 6d. The six electrons in 3d orbitals for Co^{3+} ion are first merged and appear in pairs in $3d_{xy}$, $3d_{yz}$, and $3d_{zx}$ orbitals. The $3d_{z^2}$, $3d_{x^2-y^2}$, 4s, $4p_x$, $4p_y$, and $4p_z$ orbitals for Co^{3+} ion are hybridized in the d^2sp^3 pattern and become six hybridization orbitals with no electrons distributed in regular octahedron as shown in Figure 6a,b. A $[CoSb_6]$ octahedron, as shown in Figure 6c,d, is formed in a Sb−Co coordination bond between the hybridization orbital of Co^{3+} ion and the $1-\beta$ one of Sb, and the sharing electron pair for the coordination bond is provided by the latter.

4.2. Implications of Photoemission Spectra of Skutterudites for Structural Evolution and Thermoelectric Transport Properties from $CoSb_3$ to $Ba_rIn_sCo_4Sb_{12}$. Figure 7a shows the photoemission spectra of Sb $3d_{5/2}$ and $3d_{3/2}$ core levels for $CoSb_3$ and $Ba_rIn_sCo_4Sb_{12}$, and Figure 7b−d shows the deconvolution spectra of photoemission spectra of Sb $3d_{5/2}$ core level for $CoSb_3$, $Ba_{0.25}Co_4Sb_{11.91}$, and $Ba_{0.14}In_{0.23}Co_4Sb_{11.84}$, respectively. Figure 8a shows the photoemission spectra of Co 2p and Ba 3d core levels and, and Figure 8b shows the Co 3p core level for $Ba_rIn_sCo_4Sb_{12}$. It can be seen that the photoemission spectra of Sb $3d_{5/2}$ and $3d_{3/2}$ core levels for all the investigated skutterudites are composed of double peaks, which is in good agreement with the result reported by Tang et al.[33] but obviously contradictory to the phenomenon reported by H. Anno et al.[48] The discrepancy may originate from the difference in the energy resolutions, because an apparatus with higher energy resolution was employed by us and Tang et al. The quantitative results of the photoemission spectra of the Sb $3d_{5/2}$ core level for $Ba_rIn_sCo_4Sb_{12}$ obtained by Gaussian−Lorentzian deconvolution analysis were listed in Table 2. The five deconvolution peaks 527.78, 528.95, 529.90, 530.60, and 531.30 eV of the photoemission spectra of Sb $3d_{5/2}$ core level in $CoSb_3$ are close to the reported values (527.4 ± 0.2, 529.0 ± 0.2, 530.10 ± 0.2, 531.20 ± 0.2, and 532.30 ± 0.2 eV) in $Ca_mCe_nFe_xCo_{4-x}Sb_{12}$,[33] showing that the Sb in $CoSb_3$ has five chemical states. However, the assignments for the five chemical states must be different from the explanation given by Tang et al.[33] Because all the Sb-icosahedron voids in $CoSb_3$ were not filled by any atom, the percentages of the five deconvolution peaks thus have no relation with the filling fraction. According to the bonding states in $CoSb_3$ described above, the five chemical states of Sb in $CoSb_3$ can be inferred as follows. (1) The chemical state about 527.78 eV with a content of 43.0% is assigned to the short $\beta\beta\sigma$ Sb−Sb bonds. The lowest binding energy is due to the highest density of electron cloud for the short $\beta\beta\sigma$ bonds. (2) The chemical states about 529.90 eV with a content of 30.2% and about 530.60 eV with a content of 14.9% are attributed to the long ppσ Sb−Sb bonds. The total content of 45.1% for both chemical states is very close to 43%, because the amounts of short $\beta\beta\sigma$ and long ppσ Sb−Sb bonds are in fact equal in $CoSb_3$. The higher binding energies for long ppσ Sb−Sb bonds are relative to the lower density of electron cloud compared to the short $\beta\beta\sigma$ Sb−Sb bonds. (3) The chemical state about 528.95 eV with a content of 8.9% is attributed to the Co−Sb coordination bonds. The small chemical shift can be explained in terms of the screening effect that is probably due to the hybridization of Co 3d orbitals with Sb 5p orbitals and/or strong σ-type Sb−Sb bonds in the $[Sb_4]^{4-}$ rings. (4) The chemical state about 531.30 eV with a content of 3.0% is assigned to the ppπ bonds perpendicular to the rectangular $[Sb_4]^{4-}$ ring. The highest binding energy is due to the lowest density of electron cloud for the bonds.

Compared to $CoSb_3$, three chemical states of Sb in $Ba_{0.25}Co_4Sb_{11.91}$ about 527.55, 528.75, and 529.65 eV, attributed to short $\beta\beta\sigma$ Sb−Sb bond, Co−Sb covalent bond, and long ppσ Sb−Sb bond, respectively, shifted to lower binding energies (about −0.2 eV). The chemical shifts can be explained in terms of the differences in electronegativities between constituent atoms (Ba = 0.89, In = 1.78, Co = 1.88, and Sb = 2.05). Namely, Ba filler in the Sb-icosahedron voids could bring out electron transition from Ba to Sb and result in a small enhancement in the densities of electron cloud of the chemical bonds in $[Sb_4]^{4-}$ ring. In addition, the Ba filler still caused significant increase in the content of short $\beta\beta\sigma$ Sb−Sb bond and remarkable reduction for long ppσ Sb−Sb bond. The phenomenon suggested that the rectangular $[Sb_4]^{4-}$ ring became smaller and squarer when the Sb-icosahedron void was filled by a Ba atom, in accord with structural studies.[44] The photoemission spectrum of Co 3p core level for $Ba_{0.25}Co_4Sb_{11.91}$ is almost the same as that for $CoSb_3$, indicating that the Ba filler has no effect on the chemical state of Co. However, the photoemission spectra of Co 3p core level for $Ba_rIn_sCo_4Sb_{12}$ gradually shifted to higher binding energies (maximum up to 0.75 eV) as the filling fraction of In increased. The data of Sb $3d_{5/2}$ core level for $Ba_rIn_sCo_4Sb_{12}$ listed in Table 2 show that the In filler not only caused significant reduction in the content of short $\beta\beta\sigma$ Sb−Sb bond and remarkable increase of long $pp\sigma$ Sb−Sb bond but also brought out a chemical shift for two

(48) Anno, H.; Matsubara, K.; Caillat, T.; Fleurial, J.-P. *Phys. Rev. B* **2000**, *62*, 10737.

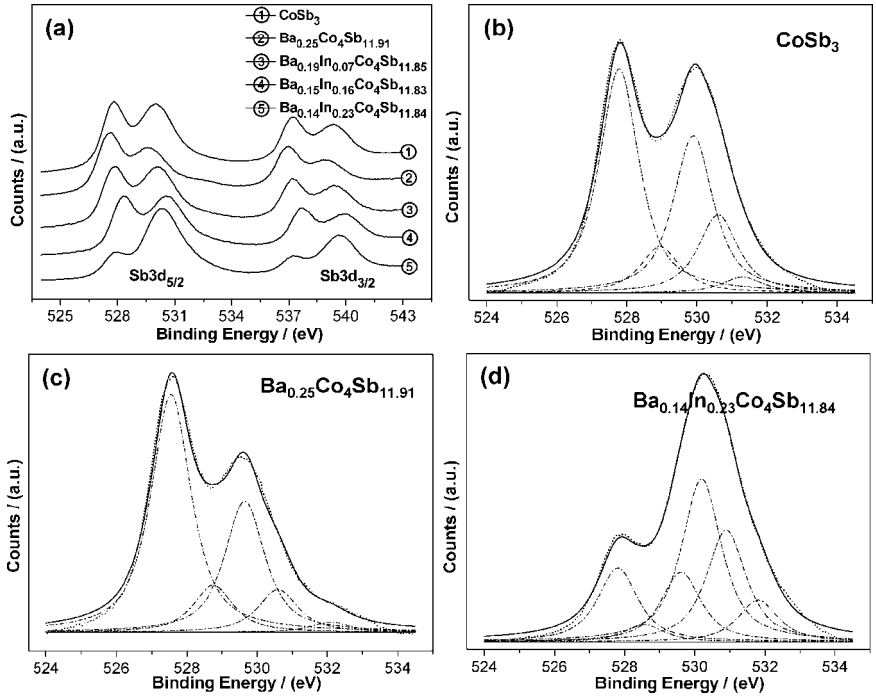

Figure 7. (a) Photoemission spectra of Sb $3d_{5/2}$ and $3d_{3/2}$ core levels for $Ba_rIn_sCo_4Sb_{12}$ and (b−d) deconvolution spectra of Sb $3d_{5/2}$ core level for $CoSb_3$, $Ba_{0.14}In_{0.23}Co_4Sb_{11.84}$, and $Ba_{0.14}In_{0.23}Co_4Sb_{11.84}$, respectively.

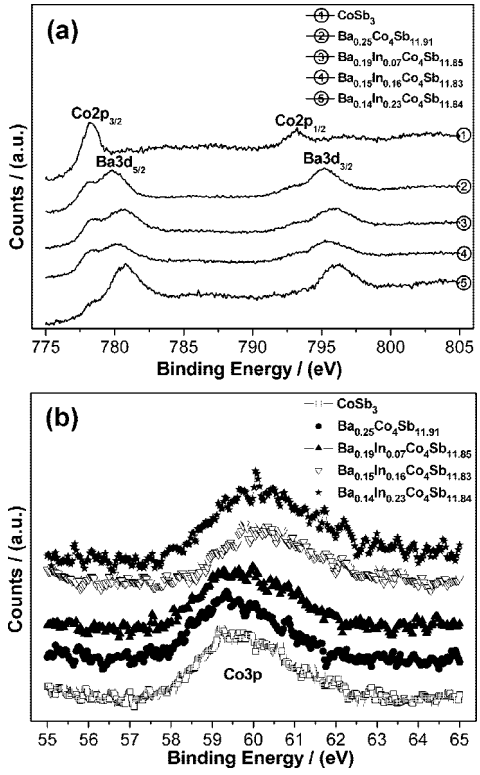

Figure 8. Photoemission spectra of (a) Co 2p and Ba 3d core levels and (b) Co 3p core level for $CoSb_3$ and $Ba_rIn_sCo_4Sb_{12}$.

chemical states of Sb about 530.20 and 530.90 eV to higher binding energies compared to that for $Ba_{0.25}Co_4Sb_{11.91}$. At the same time, there is an additional peak around 529.7 eV in $Ba_rIn_sCo_4Sb_{12}$. These phenomena show that the rectangular $[Sb_4]^{4-}$ ring became bigger and squarer and the density of electron cloud for long ppσ Sb−Sb bond decreased when the Sb-icosahedron voids were filled by In. Therefore, it can be concluded that In filler in $Ba_rIn_sCo_4Sb_{12}$ compounds brought out electron transition from Sb and/or Co to In. The reverse electron transition is attributed to the orbital hybridizations between 5p orbitals of In and 5s and/or 5p orbitals of Sb and/or 3d orbitals of Co. In general, Ba filler is divalent, and In filler is univalent in skutterudite compounds. Thus, the outer-layer electron configurations for Ba^{2+} and In^+ are $5s^24d^{10}5p^6$ and $5s^24d^{10}5p^0$, respectively. It means that In^+ may provide three 5p orbitals without electron for the orbital hybridization with 5s and/or 5p orbitals of Sb and/or 3d orbitals of Co and result in electron transition from Sb and/or Co to In, whereas Ba^{2+} cannot hybridize with Sb and/or Co because of no empty orbital for Ba^{2+}. As a consequence, the In filler results in the chemical shifts of Sb and Co in $Ba_rIn_sCo_4Sb_{12}$ to higher binding energies.

The conflicting effects of Ba and In fillers on the rectangular $[Sb_4]^{4-}$ ring are supposed to originate from the different electron transitions induced by Ba and In fillers. The charges from Sb to In are mainly from the $1-\beta$ orbital of Sb when the Sb-icosahedron voids are filled by In. As a result, the sp inhomogenous hydribization of Sb is weakened, and the rectangular $[Sb_4]^{4-}$ ring becomes bigger because of the increase in the content of long ppσ Sb−Sb bonds in the ring. On the other hand, the charges from Ba to Sb preferentially enter into the $1-\beta$ orbital of Sb when the Sb-icosahedron voids are filled by Ba. Accordingly, the sp inhomogenous hydribization of Sb is strengthened, and the rectangular $[Sb_4]^{4-}$ ring becomes smaller because of the increase in the content of short $\beta\beta\sigma$ Sb−Sb bonds in the ring. It can be easily understood that the lattice of $Ba_rIn_sCo_4Sb_{12}$ became much more disordered because of the simultaneous expansion and shrinkage of the rectangular $[Sb_4]^{4-}$ ring induced by In and Ba fillers, respectively, which may strengthen the scattering effects of carriers and phonons and efficiently reduce κ.

On the other hand, all charge-transport properties of $Ba_rIn_sCo_4Sb_{12}$ with decreasing r and increasing s mentioned above can be explained in terms of the electron transition from

Table 2. Quantitative Analysis Results of Photoemission Spectra of the Sb $3d_{5/2}$ Core Level and Their Chemical States for $Ba_rIn_sCo_4Sb_{12}$.

peak	$CoSb_3$		$Ba_{0.25}Co_4Sb_{11.91}$		$Ba_{0.19}In_{0.07}CoSb_{11.85}$		$Ba_{0.15}In_{0.16}CoSb_{11.83}$		$Ba_{0.14}In_{0.23}CoSb_{11.84}$		chemical state
	center (eV)	percent (atom %)	center (eV)	percent (atom %)	center (eV)	percent (atom %)	center (eV)	percent (atom %)	center (eV)	percent (atom %)	
Sb $3d_{5/2}$	527.78	43.0	527.55	50.7	527.79	41.5	528.28	41.7	527.80	15.6	short $\beta\beta\sigma$ Sb−Sb bond
Sb $3d_{5/2}$	528.95	8.9	528.75	10.0	529.00	10.5	529.05	3.6	528.55	3.6	Co−Sb covalent bond
Sb $3d_{5/2}$							529.70	8.5	529.61	14.6	long ppσ Sb−Sb bond
Sb $3d_{5/2}$	529.90	30.2	529.65	28.0	529.99	30.7	530.45	27.8	530.20	34.1	long ppσ Sb−Sb bond
Sb $3d_{5/2}$	530.60	14.9	530.6	9.1	530.80	15.2	531.15	15.2	530.90	23.4	long ppσ Sb−Sb bond
Sb $3d_{5/2}$	531.30	3.0	532.1	2.2	532.00	2.0	531.82	3.2	531.81	8.7	ppπ bond

Sb and Co to In due to the orbital hybridizations among In, Sb, and Co induced by In fillers. Because the electron transition from Sb to In would bring out the same amount of holes for Sb atom, the electrons from Ba to Sb were not only annihilated by the holes but also accelerated to move because of the negative effect of the holes, consequently resulting in the increase in R_H and μ_H of $Ba_{0.21}In_{0.04}Co_4Sb_{11.93}$ as well as the reduction in n compared to $Ba_{0.25}Co_4Sb_{11.91}$. However, the electrons from Ba to Sb would be fewer and fewer, and the holes being brought out by the electron transition from Sb to In would be more and more as r decreased and s increased in $Ba_rIn_sCo_4Sb_{12}$ system. Thus, the redundant holes would prevent the electrons in $Ba_rIn_sCo_4Sb_{12}$ system from moving when the holes were more than the electrons from Ba to Sb. As a result, R_H and μ_H for $Ba_rIn_sCo_4Sb_{12}$ gradually reduced, whereas n increased with decreasing r and increasing s. Therefore, we can draw the conclusion that the enhanced $\alpha^2\sigma$ and the great reduction in κ for $Ba_rIn_sCo_4Sb_{12}$ are mainly due to the orbital hybridizations induced by In filler among In, Sb, and Co.

5. Conclusion

Ba and In double-filled skutterudite compounds $Ba_rIn_sCo_4Sb_{12}$ have been fabricated by melting, quenching, annealing, and SPS methods. The EPMA data reveal that the In filler occupied the Sb-icosahedron voids more easily than the Ba filler. The electrical-transport properties and thermal conductivity were carefully examined in the temperature range of 300−850 K. It was confirmed that the thermal conductivities for $Ba_rIn_sCo_4Sb_{12}$ compounds were more remarkably reduced compared to those for Ba or In single-filled skutterudite. More interestingly, we found that filling In in Ba-filled skutterudite ($Ba_{0.3}Co_4Sb_{12}$) simultaneously enhanced the $\alpha^2\sigma$ for $Ba_rIn_sCo_4Sb_{12}$ notably. As a result, large ZT values of 1.33 and 1.34 have been obtained for $Ba_{0.15}In_{0.16}Co_4Sb_{11.83}$ and $Ba_{0.14}In_{0.23}Co_4Sb_{11.84}$ at 850 K. A model of how to form the rectangular $[Sb_4]^{4-}$ rings in $CoSb_3$ is proposed, and the five chemical states of Sb for $CoSb_3$ are reasonably assigned to different chemical bonds in the model. The quantitative analysis of photoemission spectra for $Ba_rIn_sCo_4Sb_{12}$ indicate that the In filler brought out electron transition from Sb and/or Co to In and made the $[Sb_4]^{4-}$ rings become bigger and squarer because of the orbital hybridization between In and Sb and that the Ba filler caused reverse electron transition from Ba to Sb as well as the $[Sb_4]^{4-}$ rings getting smaller and squarer because of a large difference of electronegativities between Ba and Sb. Such orbital hybridizations induced by In filler are considered to result in the significantly enhanced power factors and the great reduction of thermal conductivity of $Ba_rIn_sCo_4Sb_{12}$.

Acknowledgment. This work was support by National Basic Research Program of China (973-program, Project No 2007CB607506) and National Natural Science Foundation of China (No 10832008). Prof. W. Y. Zhao wants to thank Prof. B. L. Su from University of Namur, Belgium and Dr. S. Q. Xiao for their valuable discussions.

JA8089334